analytical chemistry

Article

Cite This: *Anal. Chem.* 2019, 91, 14066−14073

pubs.acs.org/ac

Synthesis and Application of CeO_2/SnS_2 Heterostructures as a Highly Efficient Coreaction Accelerator in the Luminol−Dissolved O_2 System for Ultrasensitive Biomarkers Immunoassay

Lei Yang,[†] Yue Jia,[†] Dan Wu,[†] Yong Zhang,[†] Huangxian Ju,[†,‡] Yu Du,[*,†] Hongmin Ma,[*,†] and Qin Wei[†]

[†]Key Laboratory of Interfacial Reaction and Sensing Analysis in Universities of Shandong, School of Chemistry and Chemical Engineering, University of Jinan, Jinan 250022, People's Republic of China

[‡]State Key Laboratory of Analytical Chemistry for Life Science, School of Chemistry and Chemical Engineering, Nanjing University, Nanjing 210023, China

Supporting Information

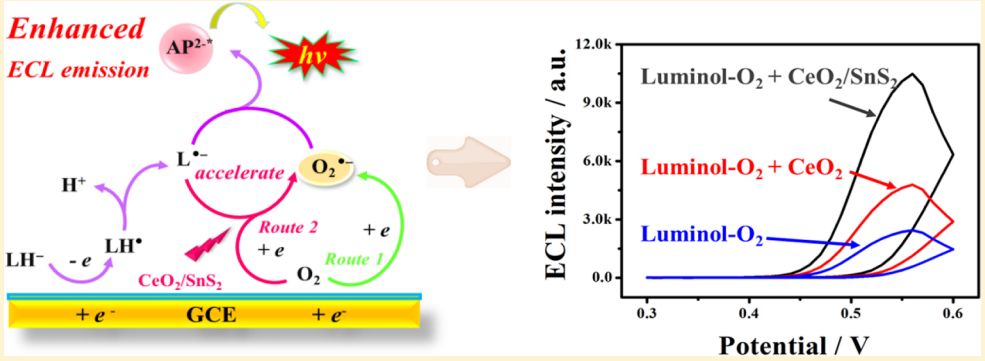

ABSTRACT: Electrocheluminescence (ECL) immunoassay amplified by coreaction accelerators has experienced major breakthroughs in ultrasensitive detection of biomarkers. Herein, CeO_2/SnS_2 heterostructures were synthesized and applied as a novel coreaction accelerator to enhance the ECL efficiency of the luminol−dissolved O_2 system for the first time. Benefiting from the well-matched lattice spacing, ultrafine CeO_2 nanoparticles (NPs) were grown in situ on layered SnS_2 nanosheets (NSs) with improved dispersion. CeO_2/SnS_2 as an electroactive substrate can remarkably accelerate the generation of abundant superoxide anion radicals ($O_2^{\bullet-}$) to react with luminol anion radical ($L^{\bullet-}$), achieving about 2-fold stronger ECL intensity than that of pure CeO_2 NPs. To avoid harsh chemical synthesis of conventional ECL labels and simplify the antibody conjugation process, ferritin (Ft) was served as a natural nanocarrier to immobilize luminol molecules (Lum@Ft) via a one-step linkage, whose protein nanocage can easily connect with the detection antibody. Moreover, a robust site-oriented immobilization strategy using HWRGWVC heptapeptide as specific capturer was further adopted to maintain the bioactivity of the capture antibody on the amine-functionalized CeO_2/SnS_2 surface, which promoted the incubation efficiency markedly. On account of this advanced sensing strategy, a brand new biosensor was constructed for the accurate detection of heart failure biomarkers, which performed with favorable linearity in the range of 0.0001−50 ng/mL and achieved the detection limit of 36 fg/mL.

Electrochemiluminescence (ECL) immunoassay has attracted tremendous attention in modern biosensing fields for protein or peptide determinations.[1,2] An advanced ECL sensing strategy rests mainly on the outstanding ECL property of applied luminous regents. With merits of nontoxic, water-soluble, and ecofriendly properties, luminol has been regarded as an extensively discussed ECL reagent in the past decades.[3,4] With the use of hydrogen peroxide (H_2O_2) as the coreactant, luminol can generate extremely strong ECL emission in alkaline solutions. However, the self-decomposition of H_2O_2 in electrolytes usually causes the unstable ECL signals of luminol during the detection, which is adverse to the reliability and accuracy of the biosensors.[5,6] As a secondary coreactant, the dissolved O_2 is usually treated as a negligible factor since the reaction efficiency of the luminol−dissolved O_2 system is much weaker than that of the luminol−H_2O_2 system.[4] Notably, the nontoxic and stable characteristics of dissolved O_2 make it a potential candidate that could eliminate the negative effects of H_2O_2 for stable luminol emission. Nevertheless, great efforts should be devoted to boost the ECL efficiency of the luminol−dissolved O_2 system to fulfill widespread applications in future bioanalysis.

Received: August 19, 2019
Accepted: October 9, 2019
Published: October 9, 2019

DOI: 10.1021/acs.analchem.9b03796
Anal. Chem. 2019, 91, 14066−14073

Scheme 1. (A) Graphical Expression of CeO_2/SnS_2–HWR Preparation, (B) Diagram of the Fabrication Process and Possible Mechanism of the Biosensor, and (C) Preparation Procedure of Lum@Ft–Ab_2 Bioconjugate

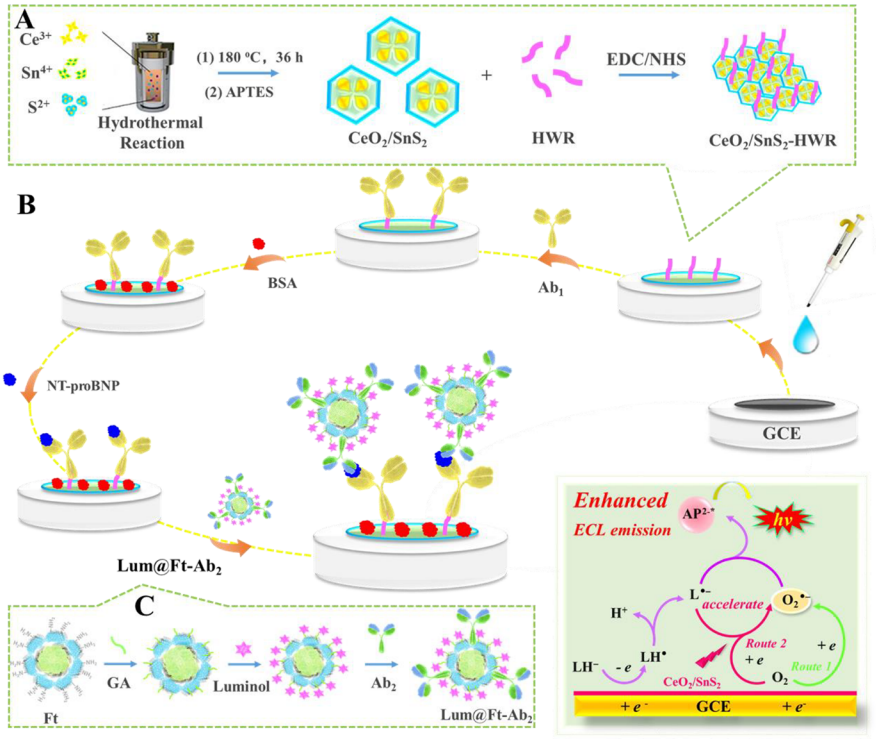

Coreaction accelerators are known as some specific substances that can significantly promote the generation of reactive intermediate radicals from coreactants to enhance the ECL efficiency of luminophores. Recently, CuS nanoparticles, silver ions, and Pt nanoparticles have all been employed as coreaction accelerators to construct ECL sensing systems.[7−9] However, most of the coreaction accelerators were applied in $S_2O_8^{2-}$-based ECL systems, with only several reports on the luminol–dissolved O_2 system. Hence, the designs and applications of novel coreaction accelerators in the luminol–dissolved O_2 system are urgently needed. Ceria (CeO_2) has drawn extensive attention due to its outstanding electrocatalytic property and oxygen storage ability in electrocatalysis, fuel cells, and sensors.[10−14] We found that CeO_2 nanoparticles (NPs) performed good signal-amplification effect on the luminol–dissolved O_2 system. It should be noted that the feasible reiterative conversion between Ce^{3+} and Ce^{4+} in CeO_2 NPs endowed themselves with high catalytic and electrical activities,[15] which could promote the generation of superoxide anion radicals ($O_2^{\bullet-}$). This effect can obtain higher production of excited-state species 3-aminophthalate (AP^{2-}*) for amplifying ECL signals. Even so, the inevitable aggregations of nanosized CeO_2 NPs adversely affected the catalytic and electrochemical properties in practical applications.

To overcome inevitable aggregation and improve electrochemical activity of CeO_2 NPs, tin disulfide nanosheets (SnS_2 NSs) as typical metal sulfides with layered structure and large specific surface area were chosen as the ideal substrate to improve CeO_2 NPs dispersion.[16−20] Crystalline analysis of hexagonal SnS_2 and cubic CeO_2 revealed the well-matched lattice spacing between the (100) lattice of SnS_2 and (111) lattice of CeO_2, which might facilitate the fabrication of CeO_2/SnS_2 heterostructures.[21] Inspired by this, we used a one-step hydrothermal reaction to prepare CeO_2/SnS_2 heterostructures, in which the CeO_2 NPs were grown in situ on SnS_2 NSs with excellent dispersion. By taking advantage of the lattice matching, the obtained CeO_2/SnS_2 heterostructures exhibited more efficient property for accelerating the generation of $O_2^{\bullet-}$ to achieve excellent ECL signal amplification, thus holding great potential in building the luminol–dissolved O_2 system for proteins and nucleic acids determination.

In view of the above, we first proposed a brand new ECL strategy using CeO_2/SnS_2 heterostructures as a coreaction accelerator to enhance the ECL efficiency of the luminol–dissolved O_2 system. First, amine-functionalized CeO_2/SnS_2 was prepared as the substrate for incubating capture antibody (Ab_1) to establish the sensing platform. To maintain the bioactivity of incubated Ab_1, HWRGWVC (HWR), a heptapeptide that can specifically capture the Fc fragment of the antibody in a site-oriented manner, was introduced onto the CeO_2/SnS_2 surface.[22] This site-oriented strategy has been demonstrated that it can improve the incubation efficiency with better maintained bioactivity than traditional methods in our previous works.[23,24] Considering the superiorities of thermal stability, pH tolerance, and enzyme mimic property, ferritin (Ft) as a biocompatible nanocarrier was utilized to immobilize luminol (Lum@Ft) via a one-step cross-linking method for the first time.[24,25] Due to the abundant amino groups on the Ft outer nanocage, the detection antibody (Ab_2) could easily be captured via an amide bond. Using natural protein as a signal label is advanced since conventional harsh chemical synthesis of nanomaterials and complex antibody conjugations can be avoided.[26] More importantly, the luminol molecules can still exhibit high ECL efficiency but with a better stability. On the basis of the above, a sandwich-type ECL biosensor using CeO_2/SnS_2–HWR–Ab_1 as the sensing platform and Lum@Ft–Ab_2 as the ECL indicator was successfully developed. Aiming at providing a practical tool

DOI: 10.1021/acs.analchem.9b03796
Anal. Chem. 2019, 91, 14066−14073

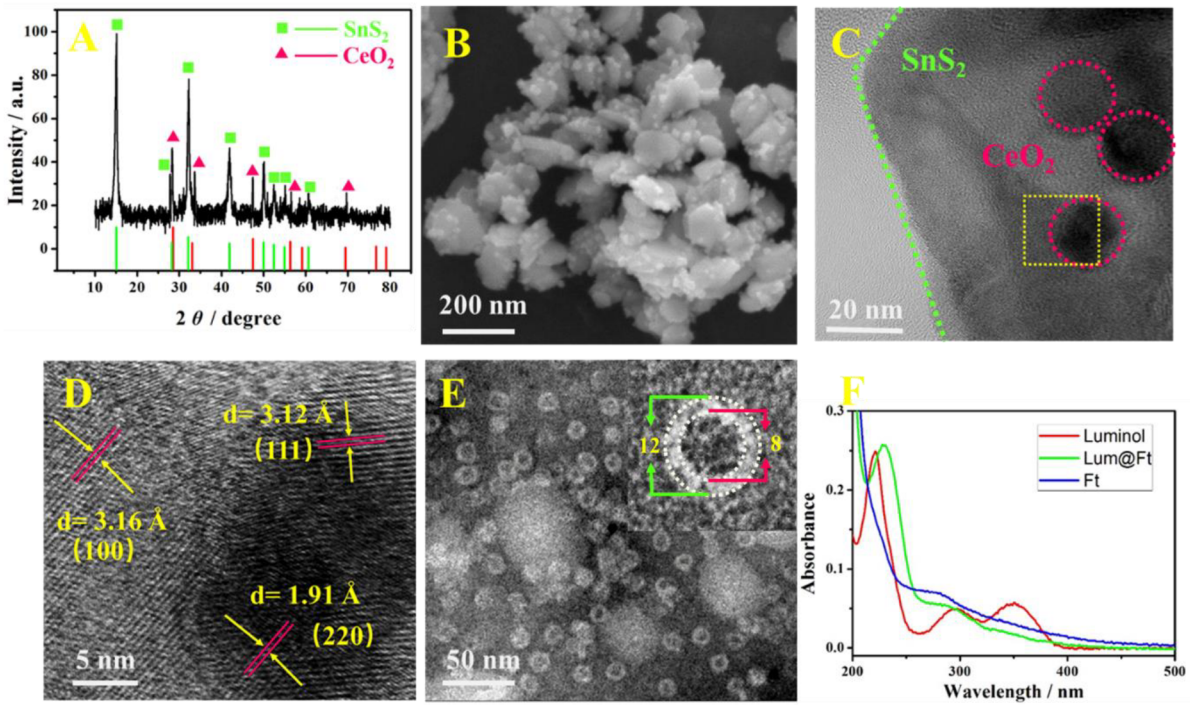

Figure 1. XRD pattern (A), SEM image (B), TEM image (C), and HRTEM image (D) of CeO_2/SnS_2 heterostructures. TEM image (E), and HRTEM image (inset) of a single Ft. UV−vis spectra (F) of Ft, luminol, and Lum@Ft.

for early clinical diagnosis of heart failure disease, a typical biomarker named N-terminal-prohormone B-type natriuretic peptide (NT-proBNP) was chosen as the analyte. The biosensor performed with favorable linearity in the range of 0.0001−50 ng/mL and achieved the detection limit of 36 fg/mL.

EXPERIMENTAL SECTION

Preparation of CeO_2/SnS_2 Heterostructures. The materials, regents, and apparatus are shown in the Supporting Information. The synthesis of CeO_2/SnS_2 heterostructures was conducted in terms of a modified method.[19] After dissolving $Ce(NO_3)_3{\cdot}6H_2O$ (0.434 g), $SnCl_4{\cdot}5H_2O$ (7.012 g), CH_3CSNH_2 (4.508 g), and 0.5 g of cetyltrimethylammonium bromide (CTAB) orderly into 40 mL of a mixture containing ultrapure water and alcohol, the resulting solution was quickly transferred into an autoclave for 36 h of reaction at 180 °C. After centrifugation and rinsing, the solid product was finally dried in vacuum at 60 °C. After sintering at 500 °C for 2 h in argon, the pristine CeO_2/SnS_2 was obtained. To realize amino functionalization, 2 mL of 3-aminopropyltriethoxysilane (APTES, 3%) was added in 10 mL of CeO_2/SnS_2 solution (2 mg/mL), and the mixture was stirred for 36 h at 60 °C. After centrifugation and washing, CeO_2/SnS_2 heterostructures covered with abundant amino groups were obtained. The above preparation is shown schematically in Scheme 1A. SnS_2 NSs were synthesized without the addition of $Ce(NO_3)_3{\cdot}6H_2O$.

Preparation of the CeO_2/SnS_2−HWR Bioconjugate. First, 2 mL of HWR (50 μg/mL) was mixed with 20 mmol of 1-(3-(dimethylamino)propyl)-3-ethylcarbodiimide hydrochloride (EDC) and 20 mmol of sulfo-*N*-hydroxysulfosuccinimide (NHS) for 15 min at 25 °C with the purpose of activating the carboxyl groups of HWR. Then, 2 mL of amine-functionalized CeO_2/SnS_2 solution (2 mg/mL) was added with the HWR solution under continuous stirring for 6 h at 4 °C. In this process, HWR could combine with CeO_2/SnS_2 via the cross-linking of EDC/NHS. After the centrifugation at 10 000 rpm, the CeO_2/SnS_2−HWR was dispersed into 1 mL of phosphate-buffered saline (PBS) (pH 7.4).

Preparation of Lum@Ft−Ab_2. First, 8 mL of Ft (50 μg/mL) solution, 200 μL of luminol (10 mmol/L), and 50 μL of glutaraldehyde (GA) (50%) were mixed in a 50 mL beaker by 2 h of stirring to finish the cross-linking (Scheme 1C). The obtained Lum@Ft was purified by dialyzing for 6 h in NaOAc solution (0.1 mol/L, pH 5.5). Then, EDC (40 mmol), NHS (10 mmol), and 100 μL of Ab_2 solution (10 μg/mL) were added orderly into the mixture for 2 h of incubation. By centrifugation at 10 000 rpm, the resulting Lum@Ft−Ab_2 was then scattered into PBS (pH 7.4) and stored at 4 °C.

Fabrication Process of the Biosensor. The fabrication diagram of the biosensor is illustrated in Scheme 1B. In the beginning, a clean glassy carbon electrode (GCE) was polished to a smooth mirror surface by 0.3 and 0.05 μm Al_2O_3 slurries. After rinsing with ultrapure water and drying in N_2, the GCE was cleaned and ready for the stepwise modification. In the beginning, 10 μL of CeO_2/SnS_2−HWR (2 mg/mL) was first coated on the clean GCE surface as the substrate. After each step below, the unabsorbed biomolecules were removed by mildly rinsing with PBS (10 mmol/L, pH 7.4). In the following step, 10 μL of Ab_1 solution (100 μg/mL) was modified onto the CeO_2/SnS_2−HWR surface and the incubation was finished at 4 °C for 1 h. Then, 10 μL of NT-proBNP was incubated for 40 min at 37 °C. Lastly, the sandwich-type immunocomplex was formed after the modification of 10 μL of Lum@Ft−Ab_2 bioconjugate. Ultimately, the biosensor was fully established and ready for the following measurements.

ECL Measurements. Before conducting the ECL measurements, the used PBS electrolyte was pretreated by O_2 bubbling for 1 h. The ECL detection measured by an MPI-F ECL

DOI: 10.1021/acs.analchem.9b03796
Anal. Chem. 2019, 91, 14066−14073

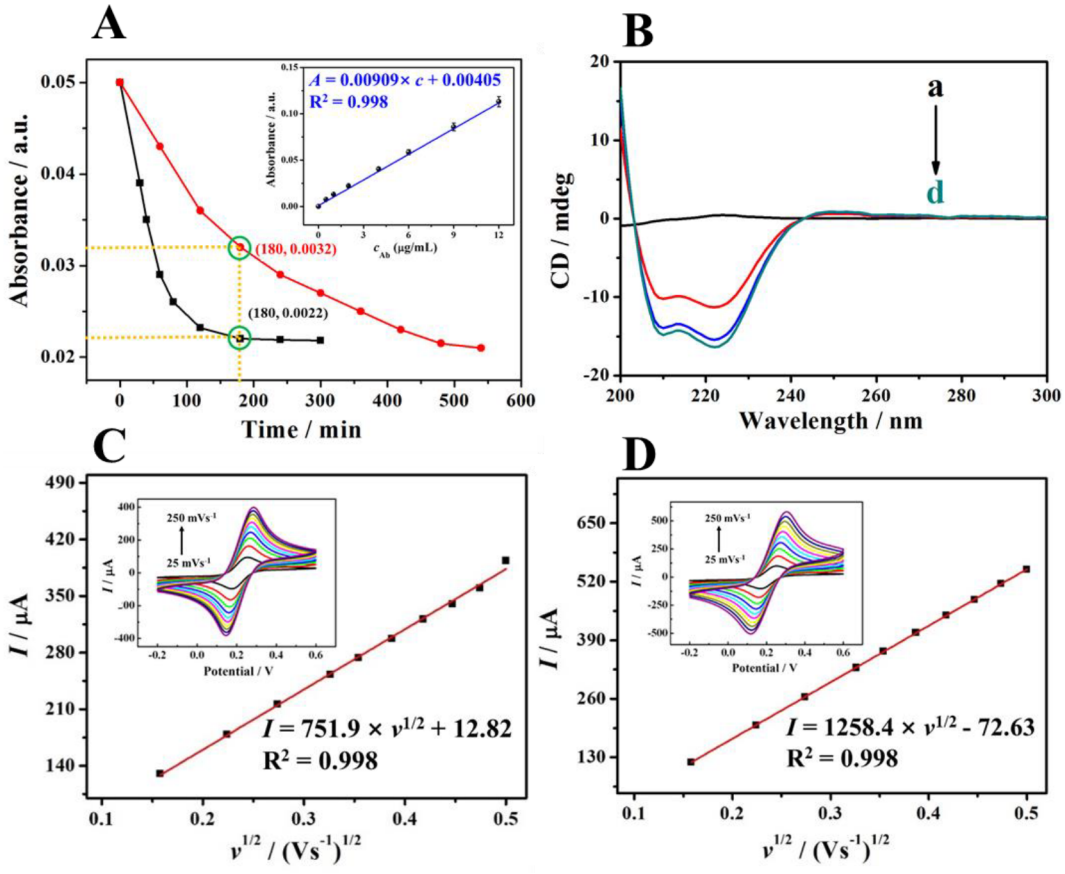

Figure 2. (A) Incubation efficiency of Ab_1 on the CeO_2/SnS_2 surface with (black curve) and without (red curve) HWR, and the calibration curve of UV−vis absorbance against antibody in a concentration range of 0−12 μg/mL (inset). (B) CD spectra of CeO_2/SnS_2−HWR (a), CeO_2/SnS_2−Ab_1 (b), CeO_2/SnS_2−HWR−Ab_1 (c), and pure Ab_1 (d). CV curves and linear relations of electrodes modified with CeO_2 NPs (C) and CeO_2/SnS_2 (D) in 5.0 mmol/L $[Fe(CN)_6]^{4-/3-}$ in the scan rate range of 25−250 mV s^{-1}.

analyzer was carried out by immersing the sensor into 10 mL of PBS (0.1 mol/L, pH 8.0). The ECL signals were obtained by scanning the electrode from 0 to 0.6 V with scan rate of 100 mV/s. The photomultiplier tube voltage was set at 600 V during the ECL detection.

RESULTS AND DISCUSSION

Characterizations of CeO_2/SnS_2 Heterostructures and Lum@Ft Bioconjugates. Compositional and morphological data of the as-synthesized CeO_2/SnS_2 heterostructures and Lum@Ft bioconjugates were characterized. The powder X-ray diffraction (XRD) patterns (Figure 1A) showed two sets of diffraction peaks that indexed to cubic CeO_2 (in red, JCPDS no. 43-1002) and hexagonal SnS_2 (in green, JCPDS no. 23-0677). By comparing with the scanning electron microscope (SEM) images in Figure 1B and Figure S1, spherical CeO_2 NPs were proved that had grown on the SnS_2 surface uniformly with fine dispersion. From the transmission electron microscopy (TEM) image of CeO_2/SnS_2, CeO_2 NPs with average diameters of about 20 nm (Figure 1C) could be seen clearly. High-resolution transmission electron microscopy (HRTEM) was further applied to obtain microstructural information on the heterostructures. As seen in Figure 1D, several lattice fringes were corresponding to the (111) and (220) lattice planes of cubic CeO_2 and the (100) planes of hexagonal SnS_2, respectively. The measured lattice spacing of the (100) plane of SnS_2 (3.16 Å) and (111) plane of CeO_2 (3.12 Å) were in good agreement with the lattice matching, which promoted the formation of CeO_2/SnS_2 heterostructures. X-ray photoelectron spectroscopy (XPS) analysis of CeO_2/SnS_2 is shown in Figure S2, which corresponded to the Ce, S, Sn, and O elements in the heterostructures. The amino functionalization of CeO_2/SnS_2 was successfully characterized by Fourier transform infrared (FT-IR) spectroscopy that is shown in Figure S3.

In addition, TEM and HRTEM images of pure Ft (Figure 1E) proved its good dispersibility with no aggregations, and the outer and inner diameters of a single Ft were about 12 and 8 nm, respectively. The UV−vis spectrum (Figure 1F) was to prove the successful cross-linking of luminol with Ft via GA. When compared with the UV−vis spectra of Lum@Ft (green curve), the characteristic peak of luminol (red curve) at 214 nm was slightly red-shifted to 236 nm, which could be explained by the conjugation enhancement between the ferritin nanocage and luminol molecules. Moreover, the characteristic peak of luminol at 347 nm faded away, which may be attributed to the consumption of the $-NH_2$ of luminol during the GA cross-linking with ferritin. Lastly, the characteristic peak of ferritin (blue curve) around 302 nm became wider, which was resulted from the successful cross-linking with luminol molecules.

Advances of HWR in the Antibody Incubation. To conduct the investigation, GCEs modified with pure CeO_2/SnS_2−HWR and CeO_2/SnS_2 were both incubated with 20 μg

DOI: 10.1021/acs.analchem.9b03796
Anal. Chem. 2019, 91, 14066−14073

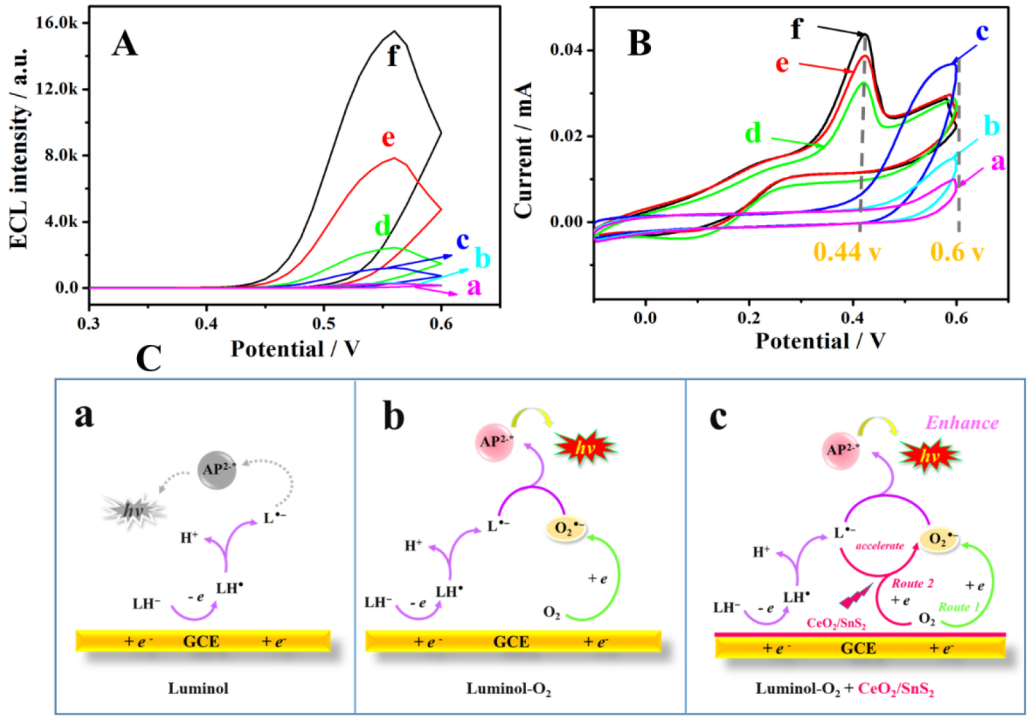

Figure 3. (A) ECL−potential. (B) CV curves of different electrodes scanned from 0 to 0.6 V: GCE modified with blank (a), CeO_2 (b), and CeO_2/SnS_2 (c) in N_2-saturated PBS (pH 8.0) solution containing 20 mmol of luminol, and GCE modified with blank (d), CeO_2 (e), and CeO_2/SnS_2 (f) in O_2-saturated PBS (pH 8.0) solution containing 20 mmol of luminol. (C) Mechanistic illustrations of luminol without any coreactants (a), the luminol−O_2 system (b), and the luminol−O_2 system using CeO_2/SnS_2 as coreaction accelerator (c).

of Ab_2 solution at 4 °C. The unhatched Ab_1 were collected after different incubation times for the UV−vis absorption test. It could be observed that the HWR curve leveled off at 180 min, proving that the antibody incubation had finished (Figure 2A). The amount of antibody incubated on the CeO_2/SnS_2−HWR surface was calculated to be 12.10 μg by using the equation $A = 0.00405 + 0.00909c$ (Ab). Similarly, the immobilized antibody on the CeO_2/SnS_2 surface was calculated to be 7.70 μg, but this incubation process did not finish until 540 min later. From the comparison it can be concluded that HWR dramatically facilitated incubation efficiency, which was an efficient strategy that can incubate large amounts of antibody in a short time.

Circular dichroism (CD) spectra have been regarded as a simple and reliable tool to characterize the maintenance of antibody bioactivity from different immobilization methods.[27] Because the specific absorption peaks of the α-helix in secondary protein structure are shown at wavelengths of 210 and 222 nm,[23,24] the antibody bioactivity from different immobilization methods can be distinguished. As shown in Figure 2B, CD spectra of CeO_2/SnS_2−HWR (curve a), CeO_2/SnS_2−Ab_1 (curve b), CeO_2/SnS_2−HWR−Ab_1 (curve c), and pure Ab_1 (curve d) are presented. The CD value of CeO_2/SnS_2−HWR−Ab_1 was similar to that of pure Ab_1, but much higher than that of CeO_2/SnS_2−Ab_1, indicating the better maintained bioactivity of Ab_1 captured on the CeO_2/SnS_2 surface by HWR. In short, the specific interaction between HWR and antibody Fc fragment is more efficient than random immobilization via amide reaction in the incubation process, underlining the advance of HWR in improving the antibody incubation efficiency with a better maintained bioactivity.

Increased Electroactive Surface Area of CeO_2/SnS_2 Heterostructures. The electrical property of CeO_2 NPs could be greatly enhanced by the supporting superiority of SnS_2 NSs, which can be verified by the increment of the electroactive surface area. To conduct the investigation, GCEs were modified with pure CeO_2 NPs and CeO_2/SnS_2 heterostructures, respectively. Then, cyclic voltammetry (CV) was measured using the commonly used $[Fe(CN)_6]^{4-/3-}$ as redox probe. The regression equations are $I = 703.9v^{1/2} + 33.82$ and $I = 1228.4v^{1/2} - 46.63$, respectively. According to the Randles−Sevcik equation[28,29]

$$I_p = \left(2.69 \times 10^5\right) AD^{1/2} n^{3/2} v^{1/2} c$$

It should be noted that I_p stands for the peak reduction current of $K_3Fe(CN)_6$, A stands for the electrochemically active area (cm^2) of electrodes modified with different materials, n stands for the number of electrons that are transported during the oxidation−reduction reaction ($n = 1$), c is the concentration of the $K_3Fe(CN)_6$ ($c = 5$ mmol/L), D is the diffusion coefficient of $[Fe(CN)_6]^{4-/3-}$ [$D = (6.70 \pm 0.02) \times 10^{-6}$ cm^2 s^{-1} at 25 °C], and v is the CV scanning rate (V/s). According to the Randles−Sevcik equation, the A values of the CeO_2 NPs modified GCE (Figure 2C) and CeO_2/SnS_2 modified GCE (Figure 2D) were calculated to be 20.21 and 35.28 mm^2, respectively.

The remarkably increased electroactive surface areas demonstrated the excellent electrochemical activity of CeO_2/SnS_2 heterostructures.

ECL Enhancement by CeO_2/SnS_2 Heterostructures. After the successful electrochemical characterization of the biosensor (Figure S4), the important role of CeO_2/SnS_2 in the luminol−dissolved O_2 system was studied. In Figure 3A, the

DOI: 10.1021/acs.analchem.9b03796
Anal. Chem. 2019, 91, 14066−14073

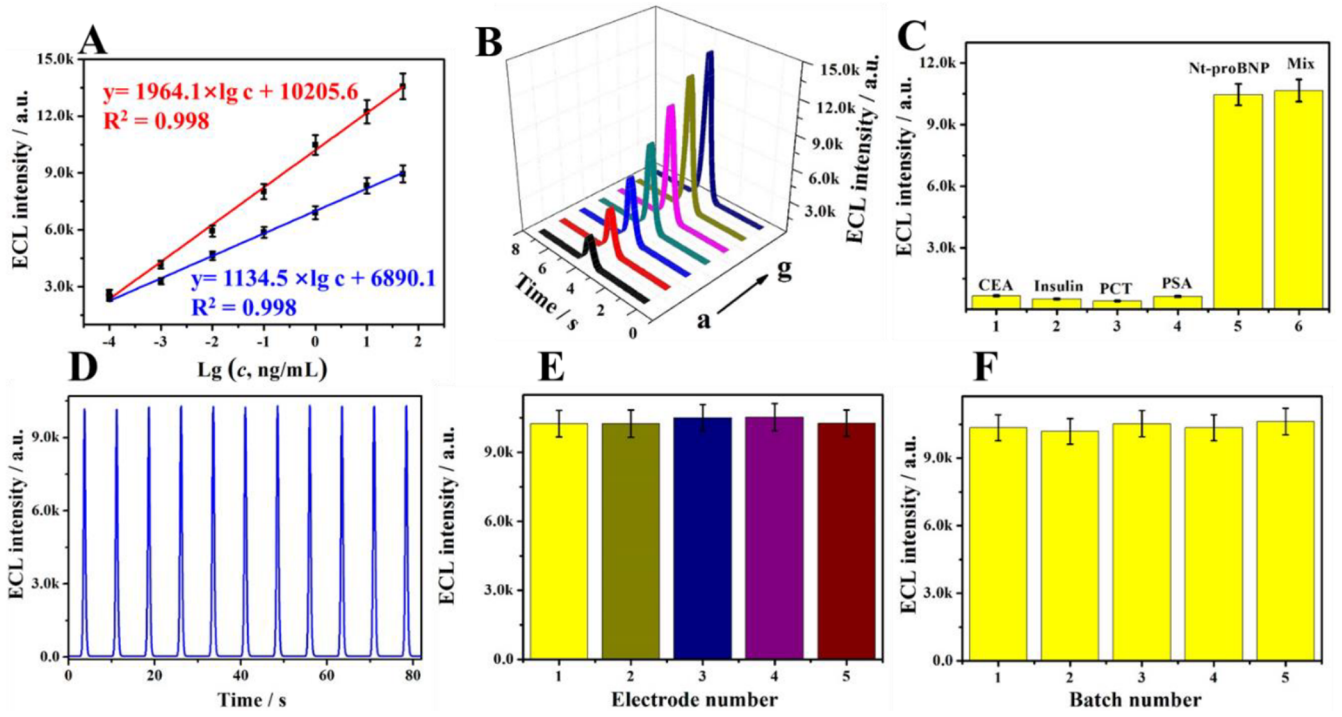

Figure 4. (A) Calibration curve of biosensors constructed with (red curve) and without (blue curve) HWR incubation to detect NT-proBNP in different concentrations: (a) 100 fg/mL, (b) 1 pg/mL, (c) 10 pg/mL, (d) 100 pg/mL, (e) 1 ng/mL, (f) 10 ng/mL, and (g) 50 ng/mL. (B) Corresponding ECL intensity−time curve to the red curve in panel A. (C) Selectivity of the proposed ECL biosensor. (D) Stability of the biosensor for 11 scans. (E) Reproducibility of five different electrodes in the same batch. (F) Reproducibility of the same electrode in five different batches. Error bars, SD, n = 5.

synchronous CV and ECL responses that were individually measured in different solutions are illustrated. Low ECL intensity (660 a.u.) were obtained from detecting bare GCE (curve a) in N_2-saturated luminol solution. After the modification of pure CeO_2 (2 mg/mL) and CeO_2/SnS_2 (2 mg/mL), no noticeable signal was found (curves b and c), proving that both CeO_2 and CeO_2/SnS_2 could not directly enhance the ECL emission of luminol. Nevertheless, when detecting bare GCE in the O_2-saturated luminol solution (curve d), the ECL signals were greatly increased to 2544 a.u., which indicated that the ECL emission of luminol occurred when using dissolved O_2 as coreactant. With respect to GCE/CeO_2/SnS_2 (curve f), about 2-fold stronger ECL signal (15531 a.u.) was achieved. This fact revealed that CeO_2/SnS_2 could facilitate the ECL emission of luminol, which is more efficient than pure CeO_2 NPs when using dissolved O_2 as the coreactant.

Furthermore, consistent CV curves of bare GCE, GCE/CeO_2, and GCE/CeO_2/SnS_2 tested in different solutions are displayed in Figure 3B. When detecting bare GCE in the N_2-saturated luminol solution, a distinctive anodic peak at 0.6 V was found from curve a. When GCE/CeO_2 (curve b) and GCE/CeO_2/SnS_2 (curve c) were tested in N_2-saturated PBS solution containing 20 mmol of luminol, the anodic currents were found to be increased, while no shift was found from peak potentials. When testing the bare GCE in O_2-saturated solution, the anodic peak (curve d) displayed a negative shift from 0.6 to 0.44 V, which could be regarded as the result of the reaction between luminol and O_2.[4] Then, GCE/CeO_2 and GCE/CeO_2/SnS_2 were both tested in O_2-saturated luminol solution; the current of GCE/CeO_2/SnS_2 (curve f) was found to be stronger than that of GCE/CeO_2 (curve e), which demonstrated that CeO_2/SnS_2 was more efficient than CeO_2 in enhancing the ECL efficiency of the luminol−dissolved O_2 system. All the above results verified that CeO_2/SnS_2 played a crucial role of being a highly efficient coreaction accelerator to react with O_2 to promote the ECL emission of luminol.

Possible ECL Mechanism Discussion. The possible ECL mechanism of our proposed ECL biosensor is described in Figure 3C. Due to the lack of coreactants, no efficient ECL emission of luminol could be generated (a). When dissolved O_2 was used as coreactant, $O_2^{\bullet-}$ was produced from the GCE surface which led to a fine ECL response (b). Tiron (1,2-dihydroxy-3,5-benzenedisulfonic acid disodium salt) solution, a specific $O_2^{\bullet-}$ scavenger, was utilized to further prove the existence of $O_2^{\bullet-}$ (Figure S5). Notably, as CeO_2/SnS_2 participated in the ECL emission process (c), the production of $O_2^{\bullet-}$ was remarkably promoted, which achieved excellent signal amplification. On this basis, a possible mechanism of this biosensor could be described as follows (eqs 1−7). First, large amounts of luminol anionic radicals ($L^{\bullet-}$) were generated by the electrochemical oxidation of luminol anions (LH^-). In route 1, $O_2^{\bullet-}$ could be produced by the electron change of dissolved O_2 on the electrode.[4] In route 2, H_2O_2 molecules were produced on the electrode surface, which could efficiently oxidize Ce^{3+} to form Ce^{4+} along with the extra generation of $O_2^{\bullet-}$ for ECL signal enhancement.[14,15,30] Therefore, after the efficient reaction between $O_2^{\bullet-}$ and $L^{\bullet-}$, more excited-state species of AP^{2-}* were produced for remarkable ECL emission.

$$LH^- - e^- \rightarrow L^{\bullet-} + H^+ \quad (1)$$

Route 1:

$$O_2 + e^- \rightarrow O_2^{\bullet-} \quad (2)$$

DOI: 10.1021/acs.analchem.9b03796
Anal. Chem. 2019, 91, 14066−14073

Table 1. Recovery Results Obtained from Human Serum Detection of NT-proBNP Using the Proposed ECL Biosensor

detected concn (ng/mL)	spiked concn (ng/mL)	theor concn (ng/mL)	found concn (ng/mL)	recovery/%
5.18	0.5	5.68	5.66	96.0
	3	8.18	8.13	98.3
	5	10.18	10.09	98.2
	10	15.18	15.28	101

Route 2:

$$O_2 + 2H_2O + 2e^- \rightarrow H_2O_2 + 2OH^- \quad (3)$$

$$Ce^{3+} + H_2O_2 \rightarrow Ce^{4+} + O_2^{\bullet -} \quad (4)$$

ECL emission:

$$L^{\bullet -} + O_2^{\bullet -} \rightarrow LO_2^{2-} \quad (5)$$

$$LO_2^{2-} \rightarrow AP^{2-}* + N_2 \quad (6)$$

$$AP^{2-}* \rightarrow AP^{2-} + h\nu \quad (7)$$

ECL Responses for NT-proBNP. After the optimizations of the involved experimental conditions (Figure S6), the biosensor was incubated with a series of NT-proBNP concentrations. As shown in Figure 4A (red curve), the calibration curve performed with a favorable linearity toward NT-proBNP concentration in the range from 100 fg/mL to 50 ng/mL. From this linearity, I_{ECL} = 1964.1 lg c + 10205.6 was expressed as the linear equation whose correlation coefficient was 0.993. The limit of detection (LOD) of this established biosensor was computationally determined as 36 fg/mL. To further highlight the crucial role of HWR in improving the sensitivity of biosensor, the calibration curve of a biosensor constructed without HWR is displayed in Figure 4A (blue curve) with a linear equation of I_{ECL} = 1134.5 lg c + 6890.1, R^2 = 0.998. From this comparison, the advance of HWR in improving the sensitivity could be further proved. Additionally, the analytical performance of the proposal method was compared with that of other reported methods (Table S1). As seen, it can be sure that our developed biosensor owned obvious advances in the ultrasensitive detection of NT-proBNP than other methods.

Specificity, Stability, and Reproducibility of the Biosensor. With aim of evaluating the specificity, four representative interfering proteins (10 ng/mL) in human serum including carcinoembryonic antigen (CEA), insulin, procalcitonin (PCT), and prostate-specific antigen (PSA) were detected. In Figure 4C, ECL biosensors incubated with interferences (10 ng/mL) showed negligible influences. Meanwhile, biosensors incubated with mixed samples (1 ng/mL of NT-proBNP and 10 ng/mL of interferences) also showed slight changes, suggesting that the biosensor had favorable specificity. Operating stability was investigated by scanning the electrodes for 11 cycles. The ECL intensities (Figure 4D) were found with no significant changes with an RSD of 2.19%, illustrating that the stability of the biosensor was good. Reproducibility of the biosensor was inspected by inter- and intra-assay precision. Five different ECL biosensors incubated with NT-proBNP (1 ng/mL) in the same batch were all detected (Figure 4E). Then, the same ECL biosensor incubated with PCT (1 ng/mL) was detected in five different batches (Figure 4F). The RSDs of intra- and interassays were 1.31% and 3.08%, respectively, indicating the favorable reproducibility of proposed ECL biosensor.

Analysis of NT-proBNP in Human Serums. Heart failure (HF), one the most common cardiovascular disorders that frequently exerts a detrimental effect on cardiovascular health, has became a major cause of human mortality.[31,32] NT-proBNP has been identified as a representative biomarker for HF early diagnosis.[33] With aim of verifying the accuracy and reliability of the biosensor, NT-proBNP was chosen as the representative biomarker for HF diagnostics. The ratio between the actual concentration (defined as added) and the detected concentration based on the linear equation (defined as found) was the recovery.[29] In Table 1, the recovery values were from 96.0% to 101% with RSD values from 0.86% to 3.24% (n = 5), highlighting its great prospects in practical applications for NT-proBNP detection in various samples.

CONCLUSIONS

In summary, CeO_2/SnS_2 heterostructures, an excellent coreactant accelerator proposed for enhancing the ECL efficiency of the luminol−dissolved O_2 system, were first synthesized and applied in a highly efficient biosensor for HF biomarker detection. Compared to pristine CeO_2 NPs, the lattice-matched SnS_2 NSs as supporter improved the dispersion of CeO_2 NPs with remarkably increased catalytic and electrical properties. Moreover, using Ft as a natural carrier to immobilize luminol and Ab_2 could perfectly avoid harsh chemical synthesis of nanomaterials and complex antibody conjugations in traditional ECL strategies, making the biosensor construction more efficient and reliable. Furthermore, polypeptide HWR greatly promoted the incubation efficiency, ameliorating the practical performance of the biosensor markedly. The biosensor achieved ultrasensitive NT-proBNP detection in the range of 0.0001−50 ng/mL with an LOD of 36 fg/mL. This strategy provides not only new insights of fabricating CeO_2-based heterostructures for enhancing the ECL efficiency of the luminol−dissolved O_2 system, but also further insights of using heptapeptide as a site-oriented immobilizer to maintain bioactivity in modern bioanalysis.

ASSOCIATED CONTENT

Supporting Information

The Supporting Information is available free of charge on the ACS Publications website at DOI: 10.1021/acs.analchem.9b03796.

Materials and regents, apparatus, molar structure of HWR, SEM image of pure SnS_2 NSs and CeO_2 NPs, FT-IR and XPS analysis of CeO_2/SnS_2, electrochemical characterization of the biosensor, Tiron test, optimization of experimental conditions, and comparison of this method with other reported methods for NT-proBNP detection (PDF)

DOI: 10.1021/acs.analchem.9b03796
Anal. Chem. 2019, 91, 14066−14073

AUTHOR INFORMATION

Corresponding Authors

*Phone: +86 531 82765730. Fax: +86 531 82765969. E-mail: sdjndxdy@163.com.

*Phone: +86 531 82765730. Fax: +86 531 82765969. E-mail: mahongmin2002@126.com.

ORCID

Dan Wu: 0000-0002-8732-5988

Yong Zhang: 0000-0002-5831-637X

Huangxian Ju: 0000-0002-6741-5302

Hongmin Ma: 0000-0002-7061-8944

Qin Wei: 0000-0002-3034-8046

Notes

The authors declare no competing financial interest.

ACKNOWLEDGMENTS

This work was supported by the National Key Scientific Instrument and Equipment Development Project of China (No.21627809), the National Natural Science Foundation of China (Nos. 21575050, 21505051, 21777056), the Special Foundation for Taishan Scholar Professorship of Shandong Province (No. ts201712052), and the Jinan Scientific Research Leader Workshop Project (2018GXRC024).

REFERENCES

(1) Zhang, Y.; Li, X.; Xu, Z.; Chai, Y.; Wang, H.; Yuan, R. *Chem. Commun.* **2018**, *54*, 10148−10151.

(2) Liang, R. P.; Yu, L. D.; Tong, Y. J.; Wen, S. H.; Cao, S. P.; Qiu, J. D. *Chem. Commun.* **2018**, *54*, 14001−14004.

(3) Zhang, H. R.; Wang, Y. Z.; Wu, M. S.; Feng, Q. M.; Shi, H. W.; Chen, H. Y.; Xu, J. J. *Chem. Commun.* **2014**, *50*, 12575−12577.

(4) Wu, F. F.; Zhou, Y.; Zhang, H.; Yuan, R.; Chai, Y. Q. *Anal. Chem.* **2018**, *90* (3), 2263−2270.

(5) Chai, Y.; Tian, D. Y.; Wang, W.; Cui, H. *Chem. Commun.* **2010**, *46*, 7560−7562.

(6) Jiang, X.; Wang, Z.; Wang, H.; Zhuo, Y.; Yuan, R.; Chai, Y. *Chem. Commun.* **2017**, *53*, 9705−9708.

(7) Song, X.; Li, X.; Wei, D.; Feng, R.; Yan, T.; Wang, Y.; Ren, X.; Du, B.; Ma, H.; Wei, Q. *Biosens. Bioelectron.* **2019**, *126*, 222−229.

(8) Lei, Y. M.; Wen, R. X.; Zhou, J.; Chai, Y. Q.; Yuan, R.; Zhuo, Y. *Anal. Chem.* **2018**, *90* (11), 6851−6858.

(9) Liu, J. L.; Tang, Z. L.; Zhuo, Y.; Chai, Y. Q.; Yuan, R. *Anal. Chem.* **2017**, *89* (17), 9108−9115.

(10) Wu, H.; Li, F.; Wang, S.; Lu, J.; Li, J.; Du, Y.; Sun, X.; Chen, X.; Gao, J.; Ling, D. *Biomaterials* **2018**, *151*, 66−77.

(11) Xia, W.; Li, J.; Wang, T.; Song, L.; Guo, H.; Gong, H.; Jiang, C.; Gao, B.; He, J. *Chem. Commun.* **2018**, *54*, 1623−1626.

(12) Turner, S.; Lazar, S.; Freitag, B.; Egoavil, R.; Verbeeck, J.; Put, S.; Strauven, Y.; Van Tendeloo, G. *Nanoscale* **2011**, *3* (8), 3385−3390.

(13) Tian, Z.; Li, J.; Zhang, Z.; Gao, W.; Zhou, X.; Qu, Y. *Biomaterials* **2015**, *59*, 116−124.

(14) Wang, J. X.; Zhuo, Y.; Zhou, Y.; Wang, H. J.; Yuan, R.; Chai, Y. Q. *ACS Appl. Mater. Interfaces* **2016**, *8* (20), 12968−12975.

(15) Wu, J.; Wang, X.; Wang, Q.; Lou, Z.; Li, S.; Zhu, Y.; Qin, L.; Wei, H. *Chem. Soc. Rev.* **2019**, *48*, 1004−1076.

(16) Seo, J.-w.; Jang, J.-t.; Park, S.-w.; Kim, C.; Park, B.; Cheon, J. *Adv. Mater.* **2008**, *20* (22), 4269−4273.

(17) Zhang, Y. C.; Li, J.; Zhang, M.; Dionysiou, D. D. *Environ. Sci. Technol.* **2011**, *45* (21), 9324−9331.

(18) Zhong, H.; Yang, G.; Song, H.; Liao, Q.; Cui, H.; Shen, P.; Wang, C. X. J. *J. Phys. Chem. C* **2012**, *116* (16), 9319−9326.

(19) Wang, Q.; Huang, Y.; Miao, J.; Zhao, Y.; Zhang, W.; Wang, Y. *J. Am. Ceram. Soc.* **2013**, *96* (7), 2190−2196.

(20) Qu, B.; Ma, C.; Ji, G.; Xu, C.; Xu, J.; Meng, Y. S.; Wang, T.; Lee, J. Y. *Adv. Mater.* **2014**, *26* (23), 3854−3859.

(21) Huang, X.; Zeng, Z.; Bao, S.; Wang, M.; Qi, X.; Fan, Z.; Zhang, H. *Nat. Commun.* **2013**, *4*, 1444.

(22) Yang, H.; Gurgel, P. V.; Williams, D. K., Jr.; Bobay, B. G.; Cavanagh, J.; Muddiman, D. C.; Carbonell, R. G. *J. Mol. Recognit.* **2009**, *23* (3), 271−282.

(23) Jia, Y.; Yang, L.; Feng, R.; Ma, H.; Fan, D.; Yan, T.; Feng, R.; Du, B.; Wei, Q. *ACS Appl. Mater. Interfaces* **2019**, *11* (7), 7157−7163.

(24) Yang, L.; Fan, D.; Zhang, Y.; Ding, C.; Wu, D.; Wei, Q.; Ju, H. *Anal. Chem.* **2019**, *91*, 7145−7152.

(25) Günther, J.; van Rijn, P.; Barbara, S. M.; Alexander, B. *Chem. Rev.* **2015**, *115* (4), 1653−1701.

(26) Tang, Z.; Wu, H.; Zhang, Y.; Li, Z.; Lin, Y. *Anal. Chem.* **2011**, *83* (22), 8611−8616.

(27) Joshi, V.; Shivach, T.; Yadav, N.; Rathore, A. S. *Anal. Chem.* **2014**, *86* (23), 11606−11613.

(28) Li, L. L.; Liu, K. P.; Yang, G. H.; Wang, C. M.; Zhang, J. R.; Zhu, J. *Adv. Funct. Mater.* **2011**, *21* (5), 869−878.

(29) Wang, H.; Yuan, Y.; Zhuo, Y.; Chai, Y.; Yuan, R. *Anal. Chem.* **2016**, *88* (4), 2258−2265.

(30) Liu, K.; Huang, X.; Wang, H.; Li, F.; Tang, Y.; Li, J.; Shao, M. *ACS Appl. Mater. Interfaces* **2016**, *8* (50), 34422−34430.

(31) Shi, L.; Li, X.; Zhu, W.; Wang, Y.; Du, B.; Cao, W.; Wei, Q.; Pang, X. *ACS Sens.* **2017**, *2* (12), 1774−1778.

(32) Zhang, H.; Han, Z.; Wang, X.; Li, F.; Cui, H.; Yang, D.; Bian, Z. *ACS Appl. Mater. Interfaces* **2015**, *7* (14), 7599−7604.

(33) Liu, Y.; Wang, H.; Xiong, C.; Chai, Y.; Yuan, R. *Biosens. Bioelectron.* **2017**, *87*, 779−785.

DOI: 10.1021/acs.analchem.9b03796
Anal. Chem. 2019, 91, 14066−14073